Basalt fiber composites for the robotic fabrication of a lunar habitat

IAC-22, A3, IPB, 9, x68749

Basalt fiber composites for the robotic fabrication of a lunar habitat

Ina Cheibas[a]*, Marlies Arnhof[b], Belinda Rich[b]

[a] *Chair of Architecture and Digital Fabrication, Department of Architecture, ETH Zürich, Stefano-Franscini-Platz 1, CH-8093 Zürich, Switzerland*, icheibas@ethz.ch
[b] *Advanced Concepts Team, ESTEC, European Space Agency, Keplerlaan 1, 2201 AZ Noordwijk, The Netherlands*, marlies.arnhof@esa.int, Belinda.Rich@esa.int,
* Corresponding Author

Abstract

This study investigates the mechanical properties of a novel composite for a lunar space habitat. The research aims to identify high-mechanical strength materials for a robotically fabricated habitat with in-situ resources. Several basalt fiber types and cementitious matrices were investigated for building a fiber-reinforced composite. The effect of the basalt fiber type - chopped, spooled, and long; and fiber percentage - 1 wt. %, 5 wt. %, and 10 wt. %; was investigated. The samples were initially exposed to a maximum lunar environmental temperature of 117°C and a medium vacuum of 0.01 atm for 24 hours. Then, these samples were tested after curing for flexural and compressive strengths until failure and cracking occurred. The 10% chopped basalt fiber and the 5% long basalt fiber composite proved the most promising combination for a high-mechanical strength composite. These composites demonstrated an improved compressive and flexural strength for the cement slurry. Moreover, this study enables the robotic fabrication potential of a mechanically resilient lunar habitat.
Keywords: Space habitat, In-Situ Resource Utilization, Lunar regolith, Basalt Fiber, Robotic Fabrication.

Acronyms

EAC-1A = European Astronaut Centre lunar regolith simulant 1
ISRU = In-Situ Resource Utilization
ESA = European Space Agency

1. Introduction

Lunar missions are an essential step in space exploration. A lunar outpost is critical for offering a testbed for science and technology development in telecommunications, human life-support, energy systems, and research in radiation and microgravity [1], [2]. This habitat can be used as a staging base in further space exploration missions, due to its strategic location and proximity to Earth, compared to other terrestrial bodies in the solar system.

A prominent approach to building lunar space habitats is by in-situ resource utilization (ISRU). Local resources such as regolith, and solar energy, are abundant on the Moon [3], [4]. These resources can be used in an automated fabrication technique to build the lunar outpost [5], [6]. The prevailing ISRU automated fabrication methods which can be used for a lunar habitat are by subtractive or additive techniques [7]. Subtractive incorporates milling, drilling, and cutting to explore the potential of lunar lava tubes as space shelters [8], [9]. Additive methods are robotic fabrication techniques, which enable rapid layered deposition of lunar soil to build a three-dimensional objects [10]. Additive is more advantageous than subtractive, because it facilitates the automated fabrication of not only shelters, but other infrastructures as well, such as landing pads, laboratories, and manufacturing facilities [11]. Additionally, additive methods have the potential to repair, restore, and add-on required performances for habitats [12]. In the past decade, the ISRU robotic fabrication potential has been demonstrated in several additive manufacturing studies for a lunar habitat. Due to the similarities with cementitious and ceramic composition of lunar regolith, the robotic fabrication techniques have been adapted from Earth-based case-studies to a lunar space habitat [13]. These methods have been using solar sintering, powder bed fusion, digital light processing, material extrusion, binder jetting, or microwave sintering [14]–[17].

Although these technologies can facilitate the fabrication of space habitats with adequate mechanical strength, a higher degree of endurance is required for withstanding and protecting from the harsh space environment [18], [19]. For example, high-compressive mechanical strength can be achieved with cementitious and ceramic materials, however, the flexural strength is yet not adequate, since these materials have limited tensile capacity and ductility [20], [21]. Consequently, to overcome these shortcomings, reinforcements are generally added to increase the load-carrying capacity and durability for large-scale structures [22]–[24]. For this reason, Earth-based robotic fabrication techniques, such as robotic AeroCrete spraying, rock printing, and mesh mold, have a great potential for a lunar space habitat. These projects display the use of reinforcements in large-scale robotic fabrication [25]–[28]. The reinforcements are essential for avoiding brittle failures at cracking, and securing a sufficiently ductile behaviour to enable stress redistribution. They can also limit deformations and crack widths, by enhancing impact resistance, and preventing fatigue [29], [30].

For a lunar space habitat, similar reinforcements concepts to conventional methods can be used in a robotic fabrication technique – such as internal or external, metallic or non-metallic, and passive or active (also known as pre-stressed) [31]. These reinforcements are selected based on their compatibility between the building material resources and the robotic fabrication method [32]–[35]. One of the prevailing methods for the robotic fabrication of cementitious materials or ceramic mixtures are fiber composites. The addition of fiber in these mixtures improves crack deflection, crack pinning, and thermal residual stresses [36]. Additionally, fiber composites are easier to control in a robotic fabrication process, compared to rigid reinforcements, through increased processing speed, parts consolidation, and improved part-to-part uniformity [37].

To date, various fibers have been tested for robotic fabrication - carbon, glass, basalt, polymer, bio-fibers (bamboo, flax, cotton, wool), and steel fibers [38]–[43]. Nevertheless, for the lunar habitat an in-situ available fiber is required. Basaltic regolith is readily available on the Moon surface [44], [45]. This basaltic soil can be used to produce thin filaments of basalt fiber [46], [47]. The fibers can have non-corrosive properties and high-mechanical strength. Unstressed basalt fibers and fabrics can maintain their integrity even up to 1250°C and down to -260°C [48]. They can withstand temperatures of 1100°C - 1200°C continuously for hours without any physical damage. Additionally, previous studies have shown enhanced mechanical properties of basalt fibers in Earth-based of cementitious composites [39], [49]–[54].

In this study, several basalt fiber composites in a cementitious matrix are investigated. These novel fibrous composites are tested to verify material strength feasibility for the additive robotic fabrication of a large-scale lunar space habitat.

2. Material and methods

Several samples have been analysed at different basalt fiber lengths and percentages in the matrix composite. The selected material used as a matrix for the fiber composite is based on a geopolymer recipe developed by Østfold University College in collaboration with the Advanced Concepts Team of the European Space Agency (ESA) [18]. The ingredients for the recipe can be readily available on the Moon, as it consists of regolith, water, sodium hydroxide, and urea obtained from astronauts' urine as a superplasticizer [55], [56]. This selected recipe is advantageous compared to other cementitious matrixes previously studied for a Moon habitat, such as sulphur "concrete" or phosphorous mixture, due to its lower water use, higher mechanical strength, and better endurance in a lunar environment [57]–[59].

2.1 Basalt fiber

The samples were manufactured by mixing the lunar cementitious base with the basalt fiber. Then the specimen were placed in rectangular Teflon prisms, and cured at the lunar environmental maximum temperature of 117°C and medium vacuum of 0.01 atm. Flexural and compressive strengths were measured after 24 h curing, within one hour after removing from the vacuum chamber at room temperature. The mechanical strength was conducted by a Zwig/Roel Z100 machine at a traversal speed of 2 mm/min.

The basalt fiber used in the experiments were manufactured and provided by Basaltex [60]. The following fiber types and distribution were investigated:

1. **Fiber type** - Chopped, spooled, and long
2. **Fiber content** – 1 wt. %, 5 wt. %, 10 wt. %

All filaments have equal diameters of 17μm and density of 2.67kg/dm³. The length differs depending on the fiber type - 6.35 mm for chopped, 90 mm for spooled (90 mm length), and 160 mm for long fibers (cut from from 600 tex/direct roving, single-end), see Fig. 1.

Fig. 1. Basalt fiber used in the samples. From left to right: chopped (left), spooled (middle), and long (right).

These basalt fibers have a high tensile strength of 2900 MPa by the ASTM D2343 standard, high elastic modulus of 85 GPa, good chemical stability, high-temperature resistance of 1350°C melting point, and reduced thermal and electrical conductivity by continuous temperature range of -250°C to 550, and 1200°C fire barrier [60]. The provided fibers were coated with a silane sizing - KV 12, KV 13 and KV 14 - which is an organic polymer in water dispersion necessary to stabilize the thread. This coating is added to secure flexible and resilient fiber properties and bonding between the basalt surface thread and the cementitious matrix [40]. However, the organic-based coating made for Earth applications is not compatible with the lunar environment due to the polymer outgassing in ultra-high vacuum [61]. For higher accuracy of the test results, the fiber sizing was removed. The estimated moisture and sizing content in the fibers is 0.5 wt. %. Thermal treatment at 400°C was applied to the basalt threads for two hours in a vacuum oven. The recorded mass loss is 0.85 wt. % for chopped, 0.51 wt. % for spooled, and 0.75wt. % for long fibers.

2.2 Cementitious matrix

The matrix recipe consists of EAC-1A lunar simulant, an aqueous sodium hydroxide solution, and urea. EAC-1A lunar simulant was selected for the experimental testing due to its chemical composition resemblance to the lunar soil, see Table 1. EAC-1A was developed by the European Astronaut Centre in Cologne and sourced from a commercial quarry in the Eifel volcanic region in Germany [62].

Table 1. Main oxides in the lunar simulants EAC-1A [62], *DNA-1 [18], JSA-2A* [63], *Apollo Highland Average chemical composition, and Apollo 17 High-Ti Mare Basalt (71055) samples* [64], *Basalt fiber* [60].

	EAC-1A	DNA-1	JSA-2A	Apollo High	Apollo 17	Basalt fiber
SiO_2	43.70	47.79	47.50	45.50	37.60	57.50
TiO_2	2.40	1.00	1.50	0.60	12.10	1.10
Al_2O_3	12.60	19.16	15.00	24.00	8.74	16.90
Cr_2O_3	-	-	-	-	0.42	-
Fe_2O_3	12.00	8.75	3.5	5.90	21.50	9.50
FeO_T	-	-	7.25	-	-	-
MgO	11.90	1.86	9.00	7.50	8.21	3.70
MnO	0.20	-	0.18	-	0.22	-
CaO	10.80	8.28	10.50	15.90	10.30	-
Na_2O	2.90	4.38	2.75	0.60	0.39	2.50
K_2O	1.30	3.52	0.80	-	0.08	0.80
P_2O5	0.60	-	0.80	-	0.05	-
Total	96.93	94.74	98.78	100	99.58	92.00

* wt. % = all in weight percent

The Recipe 1 matrix has an adequate workability, or pre-set flow property with the 1 wt. % basalt fiber content. However, the increased fiber content of 5 wt. %, and 10 wt. %, contributed to poor workability in the cementitious matrix, due to the moisture absorption as interfacial effect of the fiber. For this reason, the samples with a higher fiber content 5 wt. %, and 10 wt. % require a lower viscosity of the matrix to reach a similar workability to Recipe 1. By decreasing the alkaline solution concentration, of sodium hydroxide (NaOH), from 12M to 8M, good bonding between the basalt fiber and the ceramic matrix was achieved. Additionally, the diluted recipe contributed to avoid using additional water, a highly scare lunar resource, in the mixture. Therefore, this matrix, Recipe 2 is a variation of Recipe 1 with similar workability adjusted for a higher fiber content. Nevertheless, both recipes didn`t geopolymerized, due to a difference in mixture to the original recipe.

Table 2. Cementitious matrix recipes and fiber percentages

	EAC-1A	8M (NaOH (aq))	12M (NaOH (aq))	Urea	Basalt fiber
Recipe 1	72.5	-	25.3	2.3	1 %
Recipe 2	72.5	25.3	-	2.3	5, 10%

** wt. % = all in weight percent*

3. Experimental testing

3.1 Specimen bulk density

Lunar environment has high vacuum and fluctuating temperatures. In this environment, the cementitious matrix would undergo considerable mass loss from water outgassing. Post-exposure bulk density to vacuum and temperature is an essential value to calculate the required basalt fiber content by weight fraction in the matrix. Therefore, Recipe 1 and Recipe 2 were placed in an oven with medium vacuum and lunar maximum environmental temperatures to measure the bulk density after curing. The testing was based on the ASTM C138-17a standard [65]. The ASTM C138-17a is the most applicable method due to the absence of other standards for composites cured in lunar environmental conditions.

The samples were placed in Polytetrafluoroethylene (PTFE or Teflon) molds, selected because of the Teflon chemical resistance to the alkaline solution and ability to withstand high temperature exposure [66]. Five samples were poured for each recipe in Teflon cylinder molds of 15 mm radius and 20 mm height, see Fig. 2. They were then cured in a medium vacuum of 0.01 atm at 117°C for 24h. The weight of the samples was measured before and after vacuum exposure with an Ohaus EP613 Explorer Pro Precision balance, 610 g ± 0.001 g. The ρ bulk density was determined from the division between mass (m) and volume (V) of the sample, $\rho = m / V$. Before curing, the initial bulk density was 2.07 g/cm3, which reduced to 1.84 g/cm3 after curing. Therefore, the porosity of the samples increase when samples are cured in vacuum conditions. [67]

Fig. 2. Post-cured samples used for bulk density measurement.

3.2 Sample preparation

To prepare the samples for testing, a conceptual additive robotic fabrication was considered in a layer-by-layer deposition process. In this model, when deposited, the layer would have minimum three surface areas exposed to the lunar environment, as illustrated in Fig. 3. The Recipe 1 and Recipe 2 were initially mixed for 10 min with a 400 W power stainless steel blade. Then, basalt fiber were added to the recipes, and the specimens were set in PTFE rectangular molds of 40mm x 40mm x 160mm, to form the prismatic shape. However, due to the low workability of specimens containing 5 wt. % and 10 wt. % fiber addition, the composites need to be compacted into the mold to remove the trapped air inside the specimens. For each recipe, three specimens were cast.

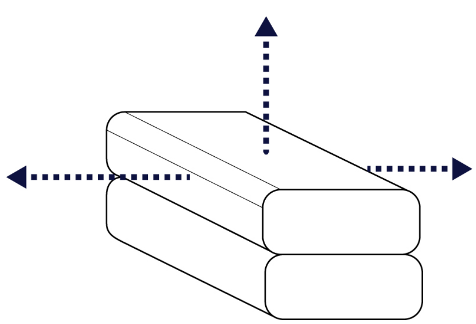

Fig. 3. Surface area exposure of the deposited layers.

The EN 196-1:2016 Standard was used as a reference for the experimental testing, due to the absence of robotic fabrication standards of fibre composites in a lunar environment [68]. However, the EN 196-1:2016 standard sample has no fiber content, and only one upper surface area is exposed to the outdoor environment. This one surface area exposure is not accurate enough for a lunar robotic fabrication scenario. The likelihood of minimum three surface area of the layer would be exposed to water outgassing. This exposure brings considerable layer deformation that can impact substantially the flexural and compressive strengths of the sample. Therefore, to achieve a more accurate result, the fiber composites were initially placed in a mold to form the prisms. Then, the samples were removed from the mold to expose five surface areas to simulated lunar conditions, see Fig. 4.

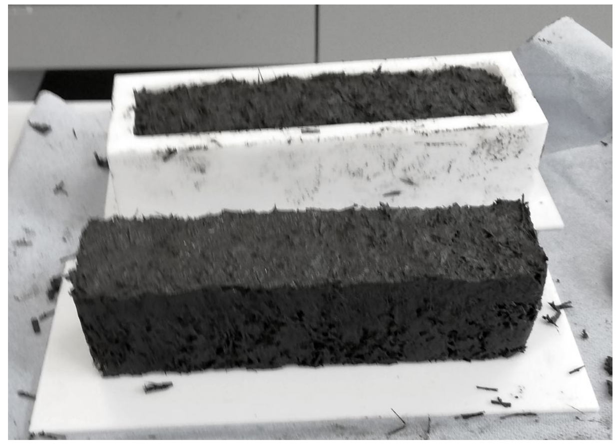

Fig. 4. Specimen preparation with teflon mold. Placement of fibre composite in the mold (upper sample) and removal from the mold (lower sample).

3.3 Environmental exposure

The specimens were placed in a Heraeus Vacuther, provided for the tests by the Directorate of Technology, Engineering, and Quality laboratory at European Space Research and Technology Centre in ESA. The samples were placed on 3 mm PTFE plates and cured in the vacuum chamber for 24h at 117°C lunar maximum temperature and 0.01 atm medium vacuum, see Fig. 5.

Fig. 5. Six long fiber 5 wt. % samples before curing in the vacuum chamber.

Fig. 6. Post-curing of three chopped fiber samples with 10 wt. % fiber content.

The exposure time of 24 hours was selected to test the initial curing phase of the composite and measure if the post-extrusion strength of the fiber composite is suitable for layer-by-layer deposition, see Fig. 6. These values are essential for identifying the fabrication potential of the deposited layers mechanical strength.

After vacuum curing, all samples' height, width and length were measured with a Stainless Steel Digital Caliper, and weight with the Ohaus EP613 Explorer Pro Precision balance. Empirical analysis showed an increase in the specimen dimensions. Additionally, the cured samples had considerable mass loss, due to water, which also contributed to decreased specimen bulk density and increased porosity.

3.4 Mechanical testing

Mechanical testing was performed for flexural and compressive strength after vacuum curing. The flexural test samples were placed on two steel supporting rolls of 10 mm diameter, and a spaced distance of 100 mm, see Fig. 7. Three samples for each recipe and fiber type were tested, with a total number of 33 samples. The average cross-section area of all specimens was 1672 mm², and an average height of 40.97 mm. Flexural strength R_f was calculated Megapascals (MPa) as follows:

$$R_f = 1.5 \cdot N \cdot l \,/\, b \cdot h^2 \qquad (1)$$

N is the load applied to the middle of the prism at fracture in Newton (N), l is the distance between support (mm), b is the length of one side of the square prism (mm), and h is the height of the prism (mm).

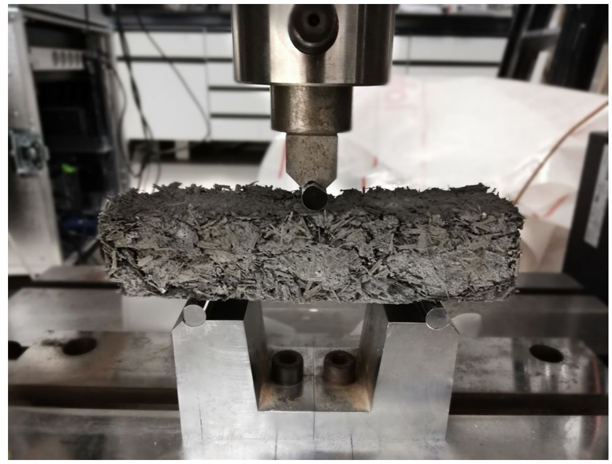

a

b

Fig. 7. Flexural testing of a) 10 wt. % chopped fiber; and b) 1 wt. % long fiber sample after critical failure.

Following the EN 196-1:2016 standard, the ruptured samples from the flexural strength test were used for compressive strength tests, see Fig. *8*. The specimens were placed on a stainless steel rectangular plate of 10 mm thick, 50 mm wide, and 50 mm long. Six samples for each recipe and fiber type have been analysed, with a total number of 66. The compressive strength R_c was calculated in Megapascals (MPa):

$$R_c = F_c \,/\, b \cdot h \qquad (2)$$

F_c is the maximum load at fracture in Newton (N), b is the length of each side of the square of the prism (mm), and h is the height of the prism (mm).

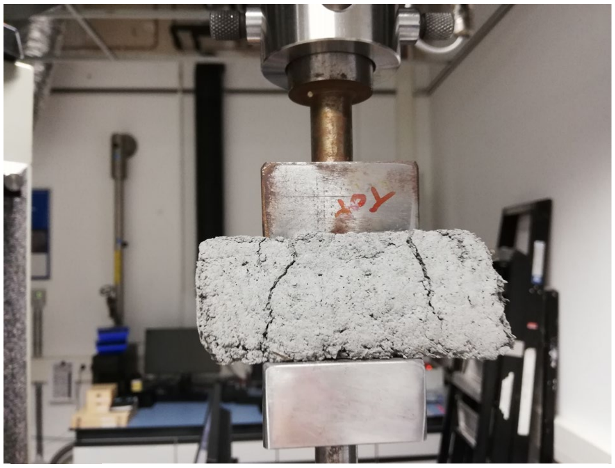

Fig. 8. Compressive strength test of 5 wt. % chopped fiber sample.

The Young`s modulus (E) in Megapascal (MPa) was calculated to determine the sample resistance to elastic deformation when compressive stress is applied. The following equation was used:

$$E = \sigma \,/\, \varepsilon \tag{3}$$

σ is the uniaxial stress force per unite area ($\sigma = F / A$), where F is the applied force in Newton (N), and A is the square area of the sample (mm^2). ε is the axial strain or proportional deformation calculated by $\varepsilon = \Delta L / L_0$, where ΔL is the length by which the sample deforms (mm), and L_0 is the initial length of the samples (mm). The deformation at break or ε elongation (%) of the samples average was calculated as well by dividing the deformed length to the initial length, $\varepsilon = \Delta L / L_0 \cdot 100$. During the mechanical testing, the Recipe 1 samples had low ductility and high brittle behaviour. In contrast, the Recipe 2 samples exhibited a much higher ductility. During both the flexural and compressive strength tests, the samples splintered off fragments before failure.

4. Results and Discussion

Exposure to prolonged vacuum and high temperatures in the vacuum oven contributed to increased porosity and mass loss of the samples. The measured average values for mass loss are 13.08% for Recipe 1, and 18.92 % for Recipe 2, see ***Fig. 9***. The mass loss effect is likely to be caused by the water outgassing in the vacuum environment. The material porosity after vacuum exposure also increased in volume, with an average increase of 13.43% for Recipe 1 and 24.38% for Recipe 2. Therefore, in the robotic fabrication process of the space habitat, the design method has to consider the increase in porosity and volume of the manufactured layer. The mass loss values are detailed in Table 3, *Appendix A*.

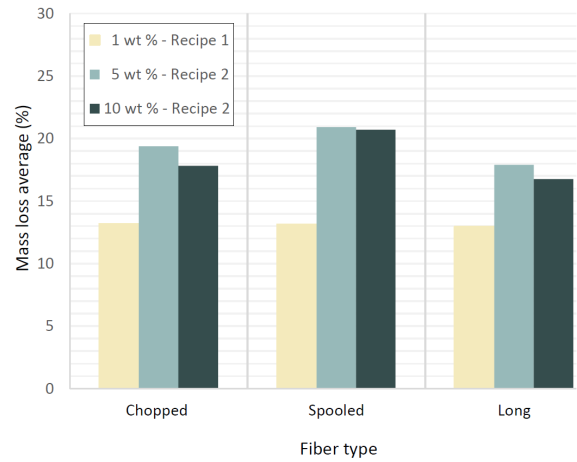

Fig. 9. Mass loss average for Recipe 1 and Recipe 2.

The investigated samples displayed an increased flexural strength with higher fiber content. Nevertheless, the values differ depending on the fiber type, see Fig. 10a. The long basalt fiber has the highest flexural strength, of 7.09 MPa for of 5 wt. %, and 7.02 MPa for 10 wt. % content. Chopped fiber of 10 wt. % has also a good outcome of 4.64 MPa. The addition of fiber also contributed to an increased compressive strength, Fig. 10b. Chopped fiber of 10% had the best behaviour with 7.38 MPa.

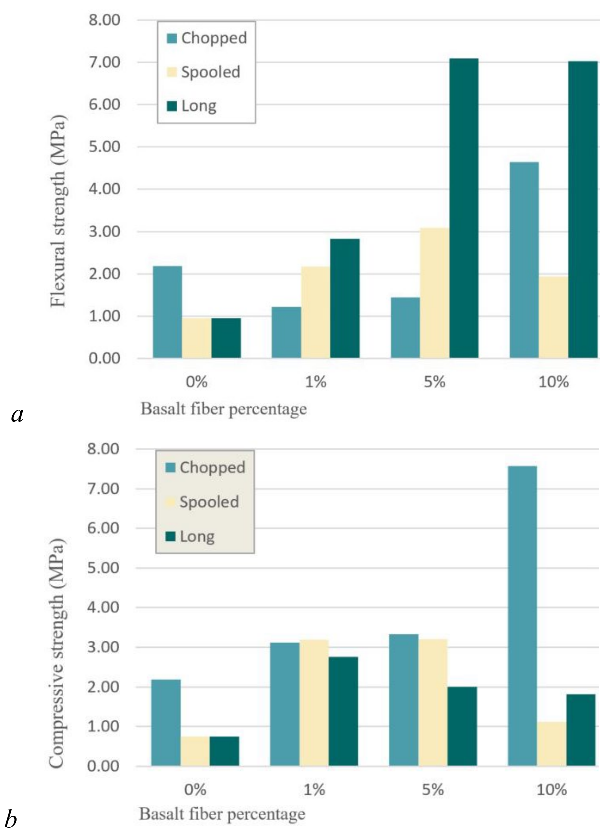

Fig. 10. a) Flexural strength of basalt fiber composite; b) Compressive strength of basalt fiber composite.

The modulus of elasticity values display an increased resistance to deformation with 1 wt. % fiber addition Fig. 11a. However, with the exception of chopped 10 wt. % fiber content, the material elasticity is significantly decreased with higher fiber content addition. Nevertheless, the main advantage of concrete-based reinforcements is the increased deformation at break, with higher content fiber addition Fig. 11b. The ability to resist changes of shape without crack deformation becomes exponentially increased for chopped and long basalt fiber. All values are detailed in **Table 4** in *Appendix B*.

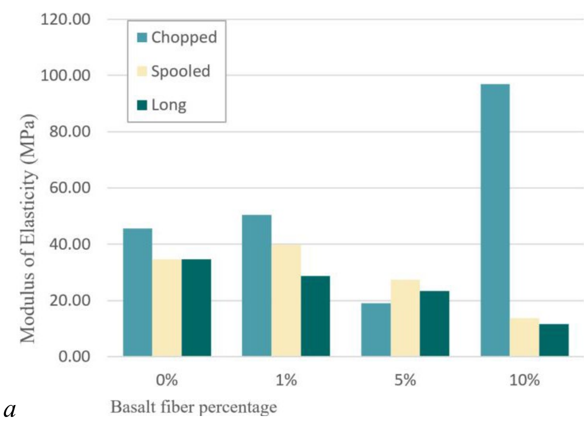

a

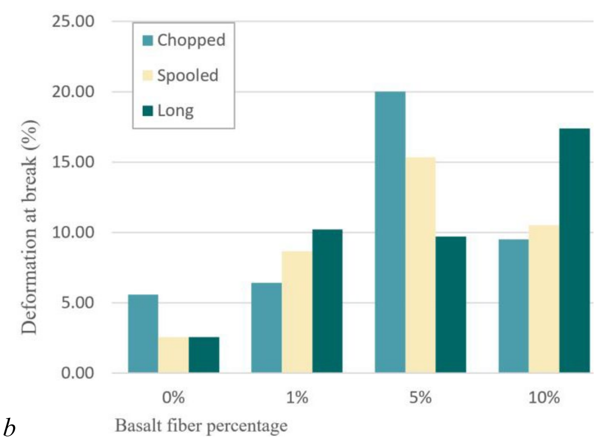

b

Fig. 11. a) Modulus of Elasticity of the fiber composite; b) Deformation at break of the fiber composite.

Although these values proved promising for space habitat manufacturing, the samples have been tested only for the initial curing of the material of 24h. Future investigation can determine the full-strength of this novel fibre composite properties by sample curing for 28-90 days. In addition, freeze-thaw effects should be examined, due to the temperature variables in a space environment. Furthermore, the increased porosity of the composite, influenced by micro-gravity and the lunar environment ultra-high vacuum is expected to adversely affect the mechanical strength.

To fabricate the composite, a suitable robotic fabrication tool can also be investigated. This tool should be able to simultaneously deposit fiber reinforcement and cementitious paste in the robotic fabrication process, to facilitate the large-scale fabrication of a sizable lunar habitat, see Fig. 12. The authors recommend augmented robotic arms and customizable nozzles with pressure pumps for fiber deposition. To manufacture the habitat, multiple layers can be deposited in traverse and Z directions similar to weaving techniques, to ensure a higher mechanical strength of the shell. When depositing the fabrication layers, the curing time and material strength are essential to secure an accurate result. This study has proven that, based on the fast curing time and high material strength, 10% chopped and long fiber can secure the robotic fabrication of high-strength composite for a lunar habitat.

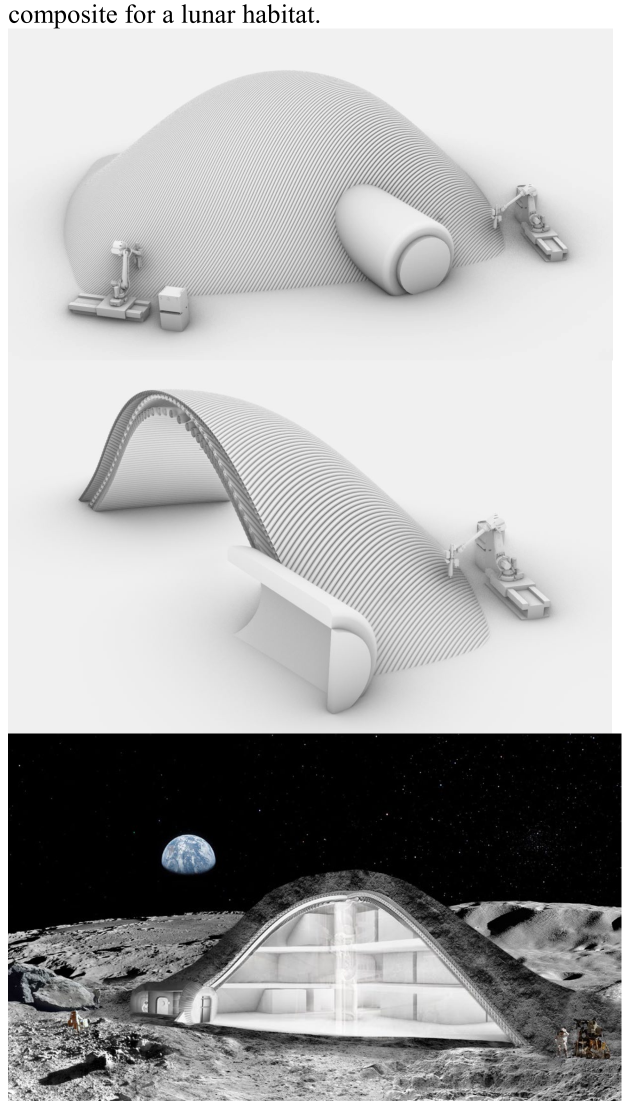

Fig. 12. Example of a large-scale lunar space habitat with robotic fabricated shell.

5. Conclusions

Several fibre composites were investigated to identify the mechanical strength in regard to flexural and compressive strength. The composites were considered for the robotic fabrication potential of a large-scale lunar space habitat.

The experimental data proved an increased mechanical strength by the addition of long and chopped basalt fiber content. With increased fiber content, higher deformation at break was detected, which is an advantageous property for redistributing the internal stresses of the space-habitat structural concept. These tests demonstrate that long basalt fiber composites contribute to higher flexural strength and deformation of 7.09 MPa, while chopped basalt fiber composites contribute to higher compressive strength of 7.38 MPa. Both fibrous composites displayed suitable mechanical strength and high potential to the robotic fabricate a sizable lunar space habitat.

This research findings are not exclusive to the robotic fabrication of a large-scale lunar habitat. Further experimental tests can be carried to investigate the fibre composite methodology for other planetary bodies or Earth-based applications.

Acknowledgements

The authors would like to acknowledge the support of the TEC (The Directorate of Technology, Engineering, and Quality) technicians at the ESTEC (European Space Research and Technology Centre) laboratory at ESA (European Space Agency). In particular to Graham Harris, Nathan Bamsey, and Advenit Makaya. As well as Aidan Cowley and Lukas Schlueter (ESA/EAC) for providing the lunar simulant EAC-1A at no charges for the ISRU experiments.

Appendix A

Table 3. Average data values for mass loss and porosity of the fibre composites

	Basalt Fiber	**Chopped Fiber**	**Spooled Fiber**	**Long Fiber**
Average mass loss (%)	1%	13.17	13.12	12.95
	5%	19.39	20.91	17.91
	10%	17.82	20.71	16.76
Material porosity (%)	1%	13.30	13.00	14.00
	5%	28.66	28.33	18.00
	10%	26.66	24.33	20.33

Appendix B

Table 4. Average data values for mechanical strength testing

Mechanical testing	**Basalt Fiber**	**Chopped Fiber**	**Spooled Fiber**	**Long Fiber**
Flexural strength (MPa)	0%	2.19	0.95	0.95
	1%	1.22	2.17	2.83
	5%	1.45	3.08	7.09
	10%	4.64	1.94	7.02
Compressive strength (MPa)	0%	2.11	0.73	0.73
	1%	3.05	3.13	2.69
	5%	2.99	3.08	1.94
	10%	7.38	1.11	1.77
Modulus of elasticity (MPa)	0%	45.67	34.64	34.64
	1%	50.40	39.84	28.65
	5%	18.97	27.37	23.44
	10%	96.92	13.66	11.66
Deformation at break (%)	0%	5.58	2.55	2.55
	1%	6.43	8.66	10.21
	5%	20.00	15.35	9.71
	10%	9.51	10.52	17.38

References

[1] H. Benaroya, *Building Habitats on the Moon: Engineering Approaches to Lunar Settlements*. Springer, 2018.

[2] H. Benaroya, *Lunar settlements*. CRC Press, 2010.

[3] G. H. Heiken, D. T. Vaniman, and B. M. French, "Lunar sourcebook-A user's guide to the moon," *Res. Support. by NASA,. Cambridge, England, Cambridge Univ. Press. 1991, 753 p. No Individ. items are Abstr. this Vol.*, 1991.

[4] G. J. Taylor and L. M. V. Martel, "Lunar prospecting," *Adv. Sp. Res.*, vol. 31, no. 11, pp. 2403–2412, 2003.

[5] S. J. Dyke, K. Marais, I. Bilionis, J. Werfel, and R. Malla, "Strategies for the design and operation of resilient extraterrestrial habitats," vol. 1159105, no. March 2021, p. 2, 2021.

[6] S. Ulubeyli, "Lunar shelter construction issues:

The state-of-the-art towards 3D printing technologies," *Acta Astronaut.*, vol. 195, no. March, pp. 318–343, 2022.

[7] H. Bier, E. Vermeer, A. Hidding, and K. Jani, "Design-to-Robotic-Production of Underground Habitats on Mars," *Spool*, vol. 8, no. 2, pp. 31–38, 2021.

[8] C. R. Coombs and B. R. Hawke, "A search for intact lava tubes on the Moon: Possible lunar base habitats," *Lunar Bases Sp. Act. 21st Century*, vol. 1, pp. 219–229, 1992.

[9] A. K. Theinat *et al.*, "Lunar lava tubes: Morphology to structural stability," *Icarus*, vol. 338, no. December 2018, p. 113442, 2020.

[10] M. Bhuvanesh Kumar and P. Sathiya, "Methods and materials for additive manufacturing: A critical review on advancements and challenges," *Thin-Walled Struct.*, vol. 159, no. July 2020, p. 107228, 2021.

[11] Y. Melodie *et al.*, "Project Olympus: Off-World Additive Construction forLunar Surface Infrastructure," *50th Int. Conf. Environ. Syst.*, no. August, p. 19, 2021.

[12] S. S. Mad Yusoh, D. Abd Wahab, H. A. Habeeb, and A. H. Azman, "Intelligent systems for additive manufacturing-based repair in remanufacturing: a systematic review of its potential," *PeerJ Comput. Sci.*, vol. 7, p. e808, Dec. 2021.

[13] A. A. Altun, F. Ertl, M. Marechal, A. Makaya, A. Sgambati, and M. Schwentenwein, "Additive manufacturing of lunar regolith structures," *Open Ceram.*, vol. 5, no. January, p. 100058, 2021.

[14] B. Rich, H. Läkk, M. Arnhof, and I. Cheibas, "Advanced Concepts for ISRU-Based Additive Manufacturing of Planetary Habitats," pp. 1–13, 2021.

[15] M. Isachenkov, S. Chugunov, I. Akhatov, and I. Shishkovsky, "Regolith-based additive manufacturing for sustainable development of lunar infrastructure – An overview," *Acta Astronaut.*, vol. 180, pp. 650–678, Mar. 2021.

[16] M. Laot, B. Rich, I. Cheibas, J. Fu, J. N. Zhu, and V. A. Popovich, "Additive Manufacturing and Spark Plasma Sintering of Lunar Regolith for Functionally Graded Materials," *Spool*, vol. 8, no. 2, pp. 7–29, 2021.

[17] S. Lim, J. Bowen, G. Degli-Alessandrini, M. Anand, A. Cowley, and V. Levin Prabhu, "Investigating the microwave heating behaviour of lunar soil simulant JSC-1A at different input powers," *Sci. Rep.*, vol. 11, no. 1, pp. 1–16, 2021.

[18] S. Pilehvar, M. Arnhof, R. Pamies, L. Valentini, and A. L. Kjøniksen, "Utilization of urea as an accessible superplasticizer on the moon for lunar geopolymer mixtures," *J. Clean. Prod.*, vol. 247, 2020.

[19] M. Liu *et al.*, "Digital light processing of lunar regolith structures with high mechanical properties," *Ceram. Int.*, vol. 45, no. 5, pp. 5829–5836, 2019.

[20] H. Toutanji, M. R. Fiske, and M. P. Bodiford, "Development and application of lunar 'concrete' for habitats," *Earth Sp. 2006 - Proc. 10th Bienn. Int. Conf. Eng. Constr. Oper. Challenging Environ.*, vol. 2006, no. 256, p. 69, 2006.

[21] V. Aulesa, "Architecture of lunar habitats," in *Exploration and Utilisation of the Moon*, 2000, vol. 462, p. 289.

[22] V. C. Li and T. Hashida, "Engineering ductile fracture in brittle-matrix composites," 1993.

[23] Y. Li and J. Li, "Relationship between fracture area and tensile strength of cement paste with supplementary cementitious materials," *Constr. Build. Mater.*, vol. 79, pp. 223–228, 2015.

[24] J. Atkinson and K. Zacny, "Mechanical properties of icy lunar regolith: Application to ISRU on the moon and mars," in *Earth and Space 2018: Engineering for Extreme Environments*, American Society of Civil Engineers Reston, VA, 2018, pp. 109–120.

[25] S. Ercan Jenny *et al.*, "Robotic Plaster Spraying: Crafting Surfaces with Adaptive Thin-Layer Printing," *3D Print. Addit. Manuf.*, vol. 9, no. 3, pp. 177–188, 2022.

[26] P. Aejmelaeus-Lindström *et al.*, "Granular Jamming of Loadbearing and Reversible Structures: Rock Print and Rock Wall," *Archit. Des.*, vol. 87, no. 4, pp. 82–87, 2017.

[27] A. Mirjan *et al.*, "Mesh Mould Prefabrication," pp. 31–36, 2022.

[28] N. Taha *et al.*, "Robotic AeroCrete A novel robotic spraying and surface treatment technology for the production of slender reinforced concrete elements," *Proc. Int. Conf. Educ. Res. Comput. Aided Archit. Des. Eur.*, vol. 3, pp. 245–254, 2019.

[29] A. Nanni, "North American design guidelines for concrete reinforcement and strengthening using FRP: Principles, applications and unresolved issues," *Constr. Build. Mater.*, vol. 17, no. 6–7, pp. 439–446, 2003.

[30] S. Brzev and K. Mitra, *Earthquake-Resistant Confined Masonry Construction*, no. December. NICEE, National Information Center of Earthquake Engineering, 2007.

[31] D. Asprone, C. Menna, F. P. Bos, T. A. M. Salet, J. Mata-Falcón, and W. Kaufmann, "Rethinking reinforcement for digital

fabrication with concrete," *Cem. Concr. Res.*, vol. 112, no. May, pp. 111–121, 2018.

[32] O. Geneidy, S. Kumarji, A. Dubor, and A. Sollazzo, "Simultaneous reinforcement of concrete while 3D printing," in *RILEM International Conference on Concrete and Digital Fabrication*, 2020, pp. 895–905.

[33] N. Hack, W. Lauer, S. Langenberg, F. Gramazio, and M. Kohler, "Overcoming repetition: Robotic fabrication processes at a large scale," *Int. J. Archit. Comput.*, vol. 11, no. 3, pp. 285–300, 2013.

[34] N. Hack, W. Lauer, F. Gramazio, and M. Kohler, "Mesh Mould: Robotically Fabricated Metal Meshes As Concrete Formwork and Reinforcement," *Proc. 11th Int. Symp. Ferrocem. 3rd ICTRC Int. Conf. Text. Reinf. Concr.*, no. June, pp. 1–13, 2015.

[35] L. Martinie, P. Rossi, and N. Roussel, "Rheology of fiber reinforced cementitious materials: classification and prediction," *Cem. Concr. Res.*, vol. 40, no. 2, pp. 226–234, 2010.

[36] G. Masi, W. D. A. Rickard, M. C. Bignozzi, and A. Van Riessen, "The effect of organic and inorganic fibres on the mechanical and thermal properties of aluminate activated geopolymers," *Compos. Part B Eng.*, vol. 76, pp. 218–228, 2015.

[37] R. R. Nagavally, "Composite Materials - History, Types, Fabrication Techniques, Advantages, and Applications," *Int. J. Mech. Prod. Eng.*, pp. 25–30, 2016.

[38] H. Assaedi, T. Alomayri, F. U. A. Shaikh, and I. M. Low, *Advances in geopolymer composites with natural reinforcement*. Elsevier Ltd, 2018.

[39] F. P. Bos, E. Bosco, and T. A. M. Salet, "Ductility of 3D printed concrete reinforced with short straight steel fibers," *Virtual Phys. Prototyp.*, vol. 14, no. 2, pp. 160–174, 2019.

[40] M. Hambach, M. Rutzen, and D. Volkmer, *Properties of 3D-Printed Fiber-Reinforced Portland Cement Paste*. Elsevier Inc., 2019.

[41] H. J. Kong, S. G. Bike, and V. C. Li, "Constitutive rheological control to develop a self-consolidating engineered cementitious composite reinforced with hydrophilic poly(vinyl alcohol) fibers," *Cem. Concr. Compos.*, vol. 25, no. 3, pp. 333–341, 2003.

[42] B. Panda, S. C. Paul, L. J. Hui, Y. W. D. Tay, and M. J. Tan, "Additive manufacturing of geopolymer for sustainable built environment," *J. Clean. Prod.*, vol. 167, pp. 281–288, 2018.

[43] D. G. Soltan and V. C. Li, "A self-reinforced cementitious composite for building-scale 3D printing," *Cem. Concr. Compos.*, vol. 90, pp. 1–13, 2018.

[44] C. M. Pieters, "Composition of the lunar highland crust from near-infrared spectroscopy," *Rev. Geophys.*, vol. 24, no. 3, pp. 557–578, 1986.

[45] L. A. Taylor, A. Patchen, R. G. Mayne, and D. H. Taylor, "The most reduced rock from the moon, Apollo 14 basalt 14053: Its unique features and their origin," *Am. Mineral.*, vol. 89, no. 11–12, pp. 1617–1624, 2004.

[46] D. Pico, A. Lüking, A. B. Sempere, and T. Gries, "Moon Basalt fiber--preliminary feasibility study," *Inst. für Textiltechnik der RWTH Aachen Univ.*, 2017.

[47] S. Wilhelm and M. Curbach, "Review of possible mineral materials and production techniques for a building material on the moon," *Struct. Concr.*, vol. 15, no. 3, pp. 419–428, 2014.

[48] S. M. Wilcox, "Tensile Properties and Fatigue Behavior of Geopolymer Matrix Composites with Carbon Fiber Reinforcement at Elevated Temperature," 2018.

[49] E. Rill, D. R. Lowry, and W. M. Kriven, "Properties of Basalt Fiber Reinforced Geopolymer Composites," no. January 2010, pp. 57–67, 2011.

[50] J. Temuujin and B. Darkhijav, "Influence of basalt fibers on the properties of fly ash based geopolymer binder," no. August, 2016.

[51] V. Dhand, G. Mittal, K. Y. Rhee, S. J. Park, and D. Hui, "A short review on basalt fiber reinforced polymer composites," *Compos. Part B Eng.*, vol. 73, pp. 166–180, 2015.

[52] D. P. Dias and C. Thaumaturgo, "Fracture toughness of geopolymeric concretes reinforced with basalt fibers," *Cem. Concr. Compos.*, vol. 27, no. 1, pp. 49–54, 2005.

[53] W. M. Kriven, J. L. Bell, and M. Gordon, "Microstructure and microchemistry of fully-reacted geopolymers and geopolymer matrix composites," *Ceram. Trans.*, vol. 153, pp. 227–250, 2004.

[54] S. S. Musil, G. P. Kutyla, and W. M. Kriven, "The effect of basalt chopped fiber reinforcement on the mechanical properties of potassium based geopolymer," in *Ceram. Eng. Sci. Proc*, 2012, vol. 33, no. 10, pp. 31–42.

[55] S. Li and R. E. Milliken, "Water on the surface of the Moon as seen by the Moon Mineralogy Mapper: Distribution, abundance, and origins," *Sci. Adv.*, vol. 3, no. 9, pp. 1–12, 2017.

[56] D. Putnam, "Composition and concentrative properties of human urine," *NASA Contract. Reports*, no. July, 1971.

[57] G. Cesaretti, E. Dini, X. De Kestelier, V. Colla, and L. Pambaguian, "Building components for

an outpost on the Lunar soil by means of a novel 3D printing technology," *Acta Astronaut.*, vol. 93, pp. 430–450, 2014.

[58] R. N. Grugel and H. Toutanji, "Sulfur 'concrete' for lunar applications - Sublimation concerns," *Adv. Sp. Res.*, vol. 41, no. 1, pp. 103–112, 2008.

[59] C. Buchner, R. H. Pawelke, T. Schlauf, A. Reissner, and A. Makaya, "A new planetary structure fabrication process using phosphoric acid," *Acta Astronaut.*, vol. 143, no. October 2017, pp. 272–284, 2018.

[60] "Basaltex." [Online]. Available: https://www.basaltex.com.mx/. [Accessed: 09-Aug-2022].

[61] C. J. William A, M. Richard S, and P. John J, "A Compilation of Outgassing Data for Spacecraft Materials."

[62] V. S. Engelschiøn *et al.*, "EAC-1A: A novel large-volume lunar regolith simulant," *Sci. Rep.*, vol. 10, no. 1, pp. 1–9, 2020.

[63] J. Schleppi, J. Gibbons, A. Groetsch, J. Buckman, A. Cowley, and N. Bennett, "Manufacture of glass and mirrors from lunar regolith simulant," *J. Mater. Sci.*, vol. 54, no. 5, pp. 3726–3747, 2019.

[64] L. Sibille, P. Carpenter, R. Schlagheck, and R. A. French, "Lunar regolith simulant materials: recommendations for standardization, production, and usage," 2006.

[65] "Standard Test Method for Density (Unit Weight), Yield, and Air Content (Gravimetric) of Concrete," West Conshohocken, Pennsylvania United States.

[66] R. Renaud and R. L. LeRoy, "Separator materials for use in alkaline water electrolysers," *Int. J. Hydrogen Energy*, vol. 7, no. 2, pp. 155–166, 1982.

[67] S. Pilehvar, M. Arnhof, A. Erichsen, L. Valentini, and A. L. Kjoniksen, "Investigation of severe lunar environmental conditions on the physical and mechanical properties of lunar regolith geopolymers," *J. Mater. Res. Technol.*, vol. 11, pp. 1506–1516, 2021.

[68] "EN 196-1:2016 - Methods of testing cement - Part 1: Determination of strength." [Online]. Available: https://standards.iteh.ai/catalog/standards/cen/37b8816e-4085-4dcc-a642-a383d9bddd6c/en-196-1-2016. [Accessed: 09-Aug-2022].